

Fine-Grained Vehicle Perception via 3D Part-Guided Visual Data Augmentation

Feixiang Lu, Zongdai Liu, Hui Miao, Peng Wang, Liangjun Zhang, Ruigang Yang, *Senior Member, IEEE*, Dinesh Manocha, *Fellow, IEEE*, and Bin Zhou

Abstract—Holistically understanding an object and its 3D movable parts through visual perception models is essential for enabling an autonomous agent to interact with the world. For autonomous driving, the dynamics and states of vehicle parts such as doors, the trunk, and the bonnet can provide meaningful semantic information and interaction states, which are essential to ensure the safety of the self-driving vehicle. Existing visual perception models mainly focus on coarse parsing such as object bounding box detection or pose estimation and rarely tackle these situations. In this paper, we address this important problem for autonomous driving by solving two critical issues using visual data augmentation. First, to deal with data scarcity, we propose an effective training data generation process by fitting a 3D car model with dynamic parts to vehicles in real images and then reconstructing human-vehicle interaction scenarios. This allows us to directly edit the real images using the aligned 3D parts, yielding effective training data generation for learning robust deep neural networks (DNNs). Second, to benchmark the quality of 3D part understanding, we collect a large dataset in real world driving scenarios with vehicles in uncommon states (VUS), *i.e.* with the door or trunk opened, etc. Experiments demonstrate our trained network with visual data augmentation largely outperforms other baselines in terms of 2D detection and instance segmentation accuracy. Our network yields large improvements in discovering and understanding these uncommon cases. Moreover, we plan to release all of the source code, the dataset, and the trained model on GitHub.

Index Terms—Fine-Grained Vehicle Perception, 3D Part-Guided Data Augmentation, Vehicles in Uncommon States (VUS), Vehicle-Human Interaction (VHI), Part-Level Object Understanding, VUS Dataset.

1 INTRODUCTION

AUTONOMOUS driving (AD) has long been considered one of the most exciting technologies that artificial intelligence (AI) is expected to deliver. Parsing and analyzing moving objects in particular vehicles is an important problem in the context of AD systems. In contrast to other generic objects, vehicles are composed with articulated and movable 3D parts (*e.g.*, doors, the trunk, and the bonnet). The dynamics and states of these parts can potentially provide meaningful semantic information and interactive states of the vehicles, which are essential for ensuring the safety of the self-driving vehicle. For example, when a car parked on the shoulder of the road has its door opened, it is likely that someone will step out of the car. As a response, the autonomous vehicle should take a proper action such as slowing down or changing lanes to avoid hitting the individual. While such cases are not common, they can be dangerous or deadly if there is no understanding of such scenarios in the AD systems. As illustrated in Fig. 1, there are many such cases in real driving scenarios, and these are extremely challenging for existing AD systems to perceive and handle.

In this paper, we mainly deal with the problem of *fine-grained* vehicle perception from a single image, particularly *vehicles in uncommon states (VUS)* in AD scenarios, by providing a 2D perception model that enables detailed 3D part-level parsing and understanding for vehicles and their interaction states with humans. Specifically, the scope of “fine-grained vehicle perception” includes: 1) recognition of vehicles in common and uncommon states, 2) 2D detection, 3) instance-level segmentation, 4) dynamic part segmentation, 5) state description, and 6) interaction semantics

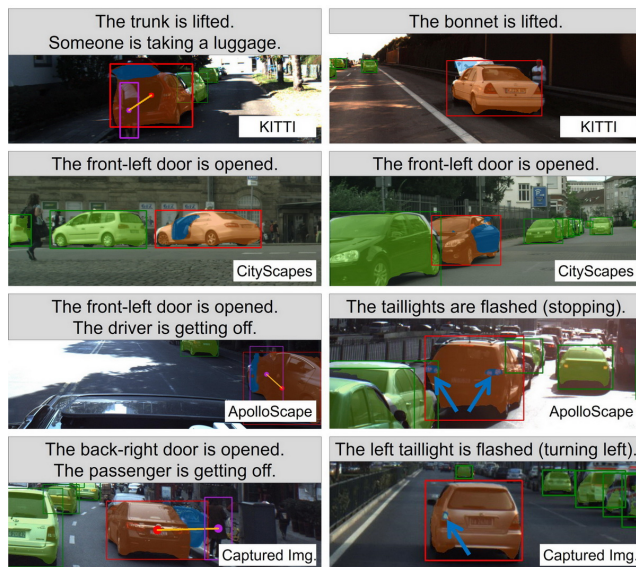


Fig. 1. Fine-grained parsing of VUS and VHI on various datasets. The results include 2D detection (red bounding box), instance segmentation (orange mask), dynamic part segmentation (blue mask), and state description. In addition, we detect the human (pink bounding box) as he or she interacts with the vehicle (yellow line). Note that the common-state vehicles are in green.

between vehicles and humans. Figs. 1, 13, 16, 17 show the results of fine-grained perception. Prior works in this area have studied one or two tasks such as 2D detection (*e.g.*, [1], [2]), semantic/instance level segmentation (*e.g.*, [3])

and part level segmentation (*e.g.*, [4]). Although these state-of-the-art (SOTA) methods have achieved good results for vehicle perception, there are many challenges with respect to uncommon vehicle identification, dynamic part segmentation, and “*vehicle-human*” interaction (VHI) semantics. In summary, the limitations of these prior works are in four aspects: 1) they are unable to recognize the VUS cases; 2) the results of detection and segmentation are not accurate due to the dynamic/movable parts; 3) it is difficult to parse the VHI semantics which can provide more information for planning and decision modules of AD systems; 4) high coupling between the training data and network. In other words, it is difficult to train a network to perform 6 perception tasks using a uniform dataset.

To achieve fine-grained vehicle perception, we evaluated many popular AD datasets, including KITTI [5], CityScapes [6], ApolloScape [7], and ApolloCar3D [8]. As shown in Fig. 1, we first find cases where a car has a part moved in real driving scenarios. Second, we determine that the number of cases is too scarce, *e.g.*, only tens within 15,000 images in KITTI, to train an effective model for fine-grained 3D part understanding. The most common strategy for generating enough training data is manually crowd sourcing large numbers of real images [9], which is labor intensive, however, other solutions such as obtaining a dataset with a simulated environment and computer graphics [10], [11], [12] will produce strong domain gaps between vehicle and scene appearances and realistic scenarios.

1.1 Main Contributions

We present a novel approach for fine-grained vehicle perception from a single image, particularly *vehicles in uncommon states* (VUS). This includes a new method for data augmentation and two efficient networks for vehicle parsing. The key aspect of our method is the 3D part-guided data augmentation strategy, which first fits a 3D vehicle geometric model with dynamic parts in images and then re-renders the edited car with re-configured parts and a realistic texture. Specifically, we adopt models from the ApolloCar3D [8] dataset, where each 2D car instance is fitted to a posed 3D model, and we define ten common dynamic parts, *i.e.* the bonnet, the trunk, four doors, two headlights, and two taillights, for each type of 3D car model. More specifically, for each part, we label its motion axis and constrain the range of movement. By sampling all the possible motion of a 3D car instance, we can automatically edit the 2D car instance from images, yielding a large number of training samples.

We further observe that humans always interact with the vehicle parts (*e.g.*, getting out of the car, taking luggage out of the open trunk, etc.). To enhance the fidelity of the synthetic data, we further generate *vehicle-human interaction* (VHI) data. Specifically, we first reconstruct the human 3D motion sequence by fitting the SMPL [13] model to the captured RGB video using the VIBE approach [14]. Then we generate a large set of texture maps based on the human database. Finally, we render the SMPL model with different texture maps to integrate the vehicle parts, yielding a large number of vehicle-human interaction samples. Experiments show that the generated VHI data can effectively improve the performance of vehicle perception.

Based on the generated data, we design and train a multi-task network to perform object understanding with fine granularity, including 2D detection, instance segmentation, dynamic part segmentation, and state description. Our deep model is significantly better at understanding vehicles in AD than models without our generated dataset. Moreover, we design a multi-stream fusion network to parse the VHI semantics, such as getting on/out, placing/removing luggage, etc.

Finally, to benchmark our perception model, to the best of our knowledge, we have constructed the first dataset with a large number of described uncommon states of vehicles in AD, *i.e.* with door or trunk open, etc., which contains 1441 labeled street-view images, 1850 car instances, and 12 defined states. We evaluate the part understanding quality extensively with the dataset and show that our network and training strategies yield large improvements (over 8% better) in discovering and understanding these uncommon cases.

In summary, our contributions include:

- We present a 3D part-guided visual data augmentation pipeline for automatic training data generation, including VUS data and VHI data, which helps to learn fine-grained vehicle perception models in AD.
- We design a multi-task network architecture that outputs both instance-level and part-level vehicle understanding. Moreover, we implement a multi-stream fusion network to parse the vehicle-human interaction semantics. These fine-grained perception results are important to the safety of autonomous vehicles.
- To benchmark our data generation strategies and network architectures, we build a large dataset with 1441 real images with fine-grained annotation of vehicles and humans in many uncommon states to demonstrate the effectiveness of our approaches.

An earlier version of this work was published in CVPR 2020 [15]. In this paper, we propose a visual data augmentation pipeline which is a complete and fully automatic solution for fine-grained vehicle perception (shown in Fig. 2). In particular, we further generate the vehicle-human interaction (VHI) data for vehicle parsing. By using both VUS and VHI data, we train a multi-stream fusion network to parse vehicle-human interaction semantics. Experiments demonstrate that our data augmentation pipeline is robust and effective. In addition, the generated VHI data can effectively improve the performance of fine-grained vehicle perception (*i.e.* the CVPR version) on 2D detection, instance-level segmentation, part-level segmentation, and state description by 3.2, 1.8, 3.1, and 1.9 percentage points, respectively. To facilitate further research and reproduce our work easily, we plan to release all of the source code, datasets, and the trained model on GitHub.

The remainder of this paper is structured as follows. Sec. 2 reviews related work. Sec. 3 introduces our data augmentation pipeline for fine-grained vehicle perception. We describe the constructed VUS dataset in Sec. 4. We compare our approach with state-of-the-art methods on VUS datasets and discuss the applications to AD in Sec. 5.

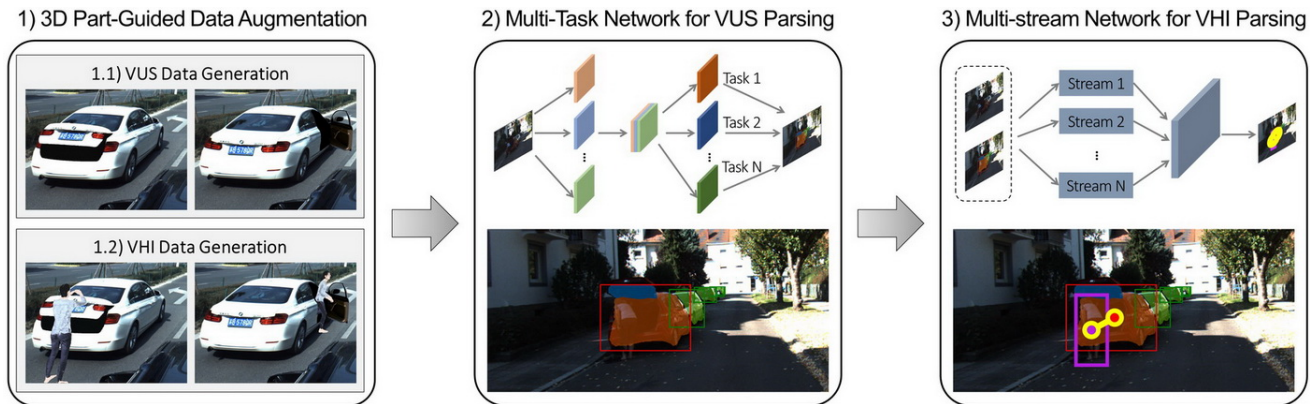


Fig. 2. Our visual data augmentation pipeline includes three main components: 1) 3D part-guided data augmentation, 2) multi-task network for VUS parsing, and 3) multi-stream network for VHI parsing. This pipeline provides a complete and fully automatic solution for fine-grained vehicle perception, which not only can generate the visual data for training, but also presents end-to-end deep networks for VUS parsing and VHI parsing.

2 RELATED WORK

Fine-grained vehicle perception is one of the central problems for autonomous driving. Our work is mostly focused on two areas: datasets and fine-grained vehicle perception. We review the related works in the following section.

2.1 Datasets for Autonomous Driving

Several datasets have been constructed and released that focus on perception in autonomous driving. The first dataset is CamVid [16], which annotates 701 images with 32 semantic classes. The later released KITTI benchmark [5] contains multiple vision tasks (*e.g.*, optical flow, 2D/3D detection). However, it mainly annotates 2D/3D bounding boxes for each car, resulting in 7481 training and 7518 test images. Recently, CityScapes dataset [6] labels vehicles with instance-level segmentation, releasing 2975 training, 500 validation, and 1525 test images. ApolloScape [7] is a large-scale AD dataset for various 2D and 3D tasks. It performs pixel-level annotations for 2D scene parsing, providing approximately 140K images. ApolloCar3D [8] is a 3D instance car dataset built from real images in driving scenes. For each car instance in a 2D image, a 3D model and corresponding 6-DoF pose are manually labeled. Moreover, there exist other real street-view self-driving datasets (*e.g.*, Toronto [17], Mapillary [18], and BDD100K [19]) and synthetic datasets (*e.g.*, SYNTHIA [20], P.F.B. [21], and Virtual KITTI [22]). However, all of these datasets only annotate common cars with 2D bounding box or semantic/instance segmentation, while vehicles in *uncommon states* are ignored (*e.g.*, opened door or trunk, flashing headlights or taillights). In an AD scenario, this information can predict further action of the vehicle, which is essential for safety.

2.2 Data Generation for Deep Network

Learning effective deep networks (*e.g.*, AlexNet [23], VGG [24], ResNet [25], and FPN [26]), depends on having a large amount of training data for each individual task. However, real data collection and annotation [7], [27], [28] are laborious. To avoid the difficulties of data labelling, synthetic data is widely used for training deep networks. Existing image synthesis techniques can be roughly divided into two

classes: 3D model rendering and 2D image “cut-paste” [29] methods. Recently, several large-scale 3D model datasets have been released, such as ShapeNet [30], ModelNet [31], and ScanNet [32]. Researchers directly render 3D models to obtain 2D images for training. However, pre-building complex realistic 3D scenes is time-consuming. Therefore, some works cut objects from images and then paste them to other backgrounds to synthesize photo-realistic training data. However, the diversity of “cut-paste” results is limited. Furthermore, it cannot handle the problem of occlusion.

Nevertheless, synthetic data improves many computer vision tasks such as optical flow [33], [34], scene flow [35], stereo [36], [37], semantic segmentation [20], [38], 3D keypoint extraction [39], viewpoint [40], object pose [41], 3D reconstruction [42], and object detection [10], [11], [12], [43]. The key problem for these works is to fix the appearance domain gap to realistic images. Domain randomization [44] is widely used for vehicle detection [11], [12], which gets the improved performance. Alhaja *et al.* [10] take advantage of the AR approach to overlay vehicle rendering results to the real street-view images, yielding augmented photo-realistic training data. Hinterstoisser *et al.* [45] show that freezing a pre-trained feature extractor can train a good object detector with synthetic data only.

2.3 Fine-Grained Parsing and Understanding

For AD, as discussed in Sec. 1, it is important to detect, segment, and parse moving objects into part-level semantics. Here, state-of-the-art (SOTA) methods often rely on detecting and understanding pipelines. Specifically, an object is first separated using detectors such as one-stage methods (*e.g.*, SSD513 [2], YOLOv3 [46]) or two-stage methods (*e.g.*, Faster-RCNN [1], Mask-RCNN [3]) and then fine-grained recognition such as part keypoints regression [8] and part segmentation [47], [48] is performed for object parts. Most recently, Lu *et al.* [4] extend the part-level pixel-wise annotation to the part state inference problem such that visual models can be more instructive. Our work follows this trend while proposes the object part-level understanding in 3D to handle uncommon cases in AD scenarios.

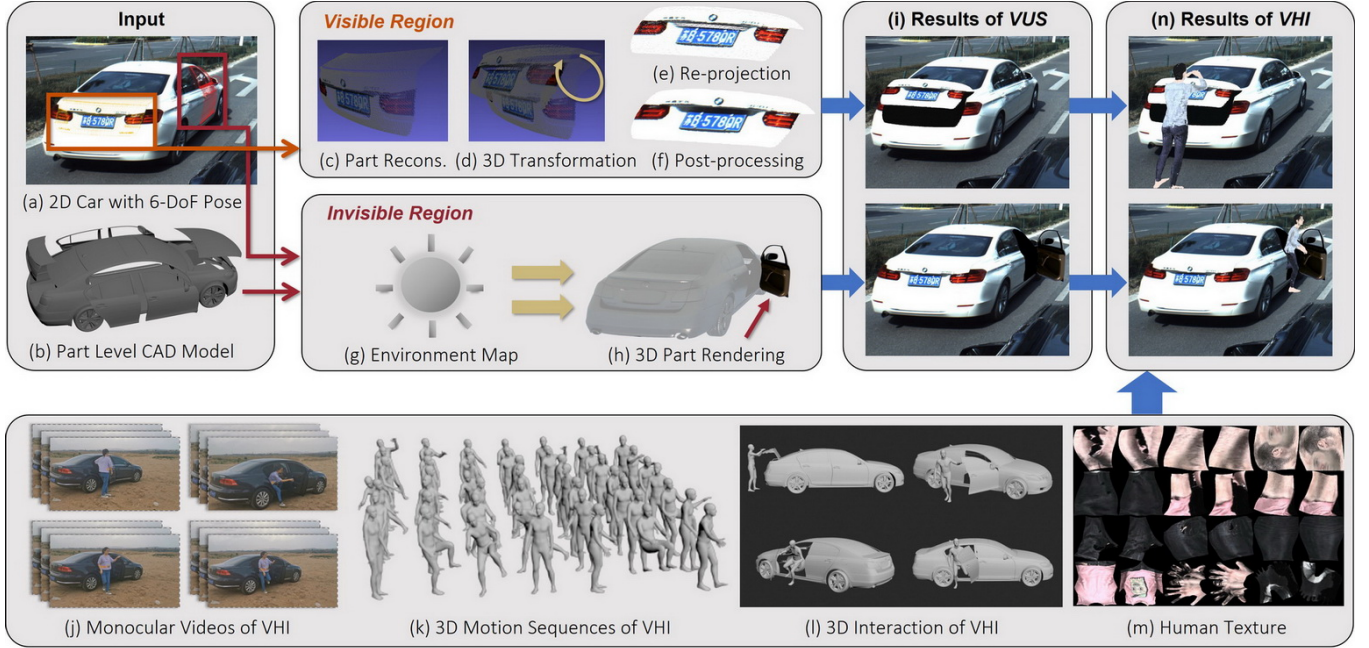


Fig. 3. This is an overview of 3D part-guided data augmentation, including VUS and VHI data generation. For the visible region of VUS data, we take the posed 2D car instances (a) and part-level CAD models (b) as input. Then we reconstruct the 3D part (c) to rotate and translate it into a new state (d). The transformed 3D part is projected onto the image space, followed by a post-processing method to refine the 2D results. For the invisible region, we use the environment map (g) to render the reverse side of the 3D part (h). (f) and (h) are augmented to the source image to generate the results of VUS (i). For VHI data augmentation, we first capture a lot of monocular videos of VHI (j), which are leveraged to estimate the 3D motion sequences (k). Next, we use the motion sequence to set the human body to virtually interact with the vehicle in 3D space (l). In addition, we build a human texture dataset (m). We randomly select the texture map to render the 3D human body of (l) to obtain the final results of VHI (n).

3 VISUAL DATA AUGMENTATION PIPELINE

In this section, we present the visual data augmentation pipeline which includes a data generation approach and two networks for data learning (shown in Fig. 2). Specifically, we first introduce the 3D part-guided data augmentation approach, which can automatically generate the VUS data and the VHI data for training (Sec. 3.1). Then we propose a novel multi-task network for fine-grained vehicle perception, including: recognition of uncommon and common vehicles, 2D detection, instance-level segmentation, dynamic part segmentation, state description (Sec. 3.2). To obtain the vehicle-human interaction semantics, we further design a multi-stream network for VHI parsing (Sec. 3.3).

3.1 3D Part-Guided Data Augmentation

As demonstrated in Fig. 3, we leverage the 3D parts to generate the VUS data and the VHI data. While most components of our data augmentation pipeline are automatic, the manual work is related to the data pre-processing, including: 1) CAD models segmentation and motion axis annotation (Sec. 3.1.1); and 2) video sequences of VHI (Sec. 3.1.2). When these data are ready, our approach is fully automatic without any human interactions from the input (source images) to output (the VUS data and the VHI data).

3.1.1 Synthesizing VUS Data

We use the 3D vehicle parts to automatically edit the source 2D images to generate various VUS samples. To achieve this goal, four essential components are required: 1) 3D part segmentation and motion axis annotation; 2) 3D transformation

and 2D projection; 3) hole filling and image filtering; and 4) invisible region generation.

Recently, Song *et al.* [8] published a 2D-3D alignment dataset, ApolloCar3D, which annotates the 3D model and 6-DoF pose for each 2D car instance. Based on the released 3D CAD models of cars, we manually segment out the *movable parts* (i.e. bonnet, trunk, and four doors) and the *semantic parts* (i.e. two headlights and two taillights). For static parts, we directly project them to obtain the corresponding 2D regions, which are further edited to yellow or red flashing effects (the third column in Fig. 4). For movable parts, we first annotate their motion axis then transform the 3D parts to guide 2D image editing. Note that the 3D models provided by ApolloCar3D are low-quality. It is difficult to obtain an appropriate texture map from a source image to perform photo-realistic rendering.

Instead, we render the 3D geometry parts to obtain a corresponding depth map D , according to the global rotation \mathbf{R}_g , translation \mathbf{t}_g , and the camera intrinsic matrix \mathbf{K} . For each 2D pixel $\mathbf{u} = (u, v)^\top$ with depth value $D(\mathbf{u})$, we convert it to acquire 3D point $\mathbf{P} = (x, y, z)^\top$ through

$$\mathbf{P} = \mathbf{R}_g^{-1} \cdot (D(\mathbf{u}) \cdot \mathbf{K}^{-1} \cdot \hat{\mathbf{u}} - \mathbf{t}_g). \quad (1)$$

Here, $\hat{\mathbf{u}}$ is a homogeneous vector: $\hat{\mathbf{u}} = (\mathbf{u}^\top | 1)^\top$.

Assuming the part is locally transformed with a 3D rotation \mathbf{R}_o along with the motion axis, the axis translates \mathbf{t}_o in the global coordinate. We compute the pixel's new position \mathbf{u}' in the image domain, which is defined as:

$$\mathbf{u}' = \left\lceil \pi \left(\mathbf{K} \cdot (\mathbf{R}_g (\mathbf{R}_o (\mathbf{P} - \mathbf{t}_o) + \mathbf{t}_o) + \mathbf{t}_g) \right) \right\rceil. \quad (2)$$



Fig. 4. The VUS data generated by our approach. The synthetic results of movable parts (*i.e.* trunk, bonnet, and four doors) are shown in the 1st column and the 2nd column. The synthetic results of semantic parts (*i.e.*, two headlights and two taillights) are shown in the 3rd column.

Here, the function $\mathbf{u} = \pi(\mathbf{P})$ performs perspective projection of $\mathbf{P} \in \mathbb{R}^3 = (x, y, z)^\top$ including dehomogenization to obtain $\mathbf{u} \in \mathbb{R}^2 = (x/z, y/z)^\top$.

Note that the transformed pixels are always sparse and noisy in the part region (Fig. 3 (e)). Here, we call the non-valued pixel a “hole”. In order to fill these holes, we perform the linear blending algorithm [49] to obtain the RGB values. In general, pixels that are close to one another will be the most similar. Thus, for consistency and efficiency, we limit the influence of the valued pixels on a particular hole to the K -nearest neighbors. The weights ω_i for each pixel \mathbf{u}_i are pre-calculated as

$$\omega_i(\mathbf{h}) = \left(1 - \|\mathbf{h} - \mathbf{u}_i\|_2 / d_{max}\right)^2 \quad (3)$$

and then normalized to sum to one. Here, d_{max} is the distance to the $(k + 1)$ -nearest pixel. We set $K = 8$ in our experiments. The RGB value of the hole h is calculated according to

$$C(\mathbf{h}) = \sum_{i=1}^K \omega_i(\mathbf{h}) \cdot C(\mathbf{u}_i). \quad (4)$$

After interpolating the non-valued pixels, we apply a bilateral filter [50] on the synthetic images. The smoothed results are shown in Fig. 3 (f) and Fig. 4.

Generating Invisible Vehicle Region

For the case of an opening car door, we can generate visually compelling results if the car is facing the camera. When the car is facing in the opposite direction, however, an opening door will introduce some invisible regions in the original image. These invisible regions can be roughly divided into two classes: one is the reverse side of the part, another is the vehicle interior (*e.g.*, seat, steering wheel, and engine). Empirically, the interior regions are always dark due to inadequate illumination. Therefore, we directly fill interior regions in with gray. While we have also attempted to use



Fig. 5. The VHI data generated by our approach. We highlight how we can synthesize various VHI cases, including getting in/out of the vehicle, placing/removing luggage, repairing the engine, and so on. These VHI cases are essential to the safety of autonomous vehicles.

random colors and patches from real images according to the experimental results, we do not find obvious differences between the options.

Compared with coloring the interior regions, coloring the reverse side of the part is rather complex. It is not appropriate to directly fill the region in with pure color. Thus, we adopt the photo-realistic rendering pipeline to generate high-fidelity results of the reverse side. Considering the low-quality models provided by ApolloCar3D, we first construct a small, expert-designed 3D model database for movable parts. Each part is designed by a professional artist with the commercial software 3dsMax. The part materials are manually labeled and the BRDF parameters are pre-defined. As shown in Fig. 3 (h), we use the environment map calculated [51] from ApolloCar3D to perform photo-realistic rendering (Fig. 3 (i)). More synthetic results of VUS are shown in Fig. 4.

3.1.2 Synthesizing VHI Data

In the real AD scenarios, vehicles in uncommon states are usually associated with human interactions (*e.g.*, getting in/out of the car, placing/removing luggage, etc.). Perceiving such “vehicle-human” interaction (VHI) cases is essential to the safety of the autonomous vehicle. However, such VHI data is not easy to capture and collect while ensuring its diversity. In this subsection, we introduce a method for automatically generating a large amount of VHI data for network training.

The VHI data augmentation pipeline is shown in Fig. 3. We first use a hand-held camera to capture 100 monocular video sequences of VHI (Fig. 3 (j)), such as getting in/out of the vehicle, placing/removing luggage, and opening the door/bonnet/trunk. Then a 3D parametric human template model (*i.e.*, SMPL-X [13]) is used to fit these videos through the VIBE approach [14], yielding the 3D human body sequences with motion parameters (Fig. 3 (k)). Next, the geometry mesh of SMPL-X is unfolded to obtain its cor-

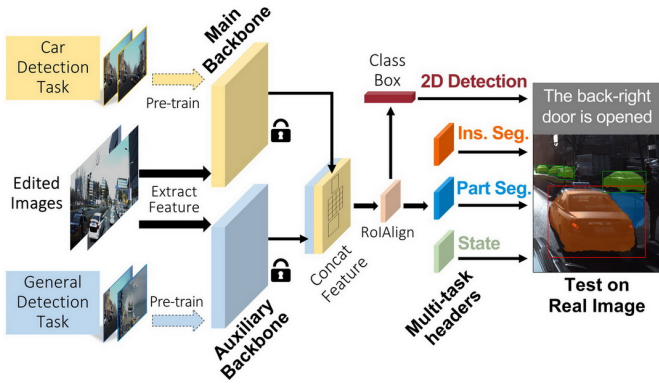


Fig. 6. We design a two-backbone network to generalize training from synthetic to real VUS data. The main backbone is pre-trained on the ApolloCar3D dataset to extract the car body features. The auxiliary backbone is pre-trained on the COCO dataset to extract the general features of the edited region (e.g. the rendered parts). We keep both backbones frozen and train our network, which can output multiple results of 2D detection, instance-level segmentation, dynamic part segmentation, and state description. In addition, we use the real-world images for testing to justify the effectiveness of our approach.

responding UV map using the Unfold3D tool. We synthesize a lot of human texture maps using the SOTA approaches (*i.e.* DensePose [52] and SURREAL [53]) to construct the texture database.

For each edited vehicle part, we select an appropriate motion sequence to guide the SMPL-X model deformed with a “coarse-to-fine” pipeline. Specifically, we first rotate and translate the global human model to match the vehicle part. Then, we adjust the body pose (*e.g.*, hand) to seamlessly interact with the vehicle parts (Fig. 3 (l)). After obtaining the posed SMPL-X model, we assign a random texture map using the constructed texture database (Fig. 3 (m)). Finally, we render the vehicle-human interaction models to generate the 2D images under the current view point (Fig. 3 (n), Fig. 5). The proposed data augmentation approach for VHI is fully automatic, and is used to generate a large amount of training data for VUS parsing (Sec. 3.2) and VHI understanding (Sec. 3.3).

3.2 Multi-Task Network for VUS Parsing

We propose a novel multi-task deep neural network architecture, as shown in Fig. 6, which is used for fine-grained object understanding. In this section, we discuss the modules of our network and training settings in detail.

3.2.1 Two Backbones

We aim to detect vehicles in uncommon states from real street-view images by training only on our synthetic images. To achieve the transferability from synthetic data to real data, there are two ResNet50-FPN [26] backbones in our network. We pre-train the *main backbone* both on the ApolloCar3D [8] benchmark and the CityScapes [6] benchmark using Mask-RCNN to extract the car body features guided by a car detection task. Simultaneously, we pre-train the *auxiliary backbone* on the COCO dataset [28] to learn the general features of the edited region (*e.g.*, the rendered parts) guided by a general detection task. Finally, we fix the

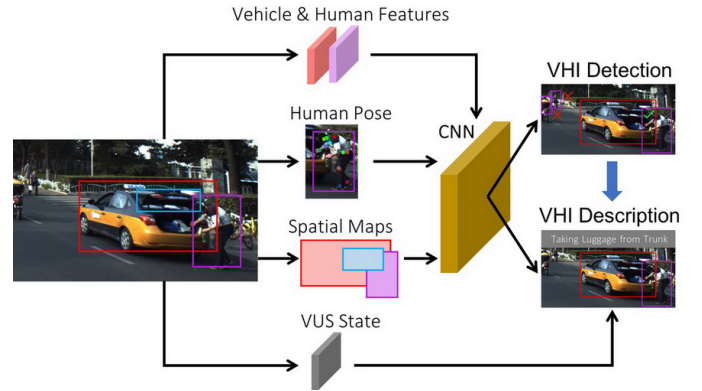


Fig. 7. The proposed deep network to parse the vehicle-human interactions. We first utilize a human stream and a vehicle stream to extract human and vehicle features, respectively. Meanwhile, spatial maps and human pose maps are also calculated. We fuse these streams to a CNN network to detect the VHI cases. The VHI detection results are combined with the VUS states (Sec. 3.2) to infer the interaction semantics between humans and vehicles.

parameters of these two backbones to train the network on the synthetic data. Indeed, experimental results in Sec. 5.5 demonstrate that we can get the optimal performance by freezing two backbones.

3.2.2 Dynamic Part Segmentation

We adopt Mask-RCNN [3] to implement the task of dynamic part segmentation. In Mask-RCNN, the mask branch outputs a Km^2 dimensional binary mask for each RoI aligned feature map, where K is the number of classes and m is the resolution. In addition, we take the dynamic part segmentation as a new channel, resulting in an output containing a $(K + 1)m^2$ binary mask. Specifically, we feed a 14×14 RoI aligned feature map to four sequential 256-d 3×3 convolution layers. A 2×2 deconvolution layer is used to up-sample the output to 28×28 . Finally, we define the L_{part} as the average of per-pixel sigmoid cross entropy loss.

3.2.3 State Description

We use a binary variable to represent the existence of the particular part state (*i.e.* 1 for existence and 0 for others). Then, we define the “part state vector” as a concatenation of all the binary variables. Our method regresses the part state vector through the sequential convolution layers and a fully connected layer in the mask branch. Similarly, we define the L_{state} as the average sigmoid cross entropy loss.

3.2.4 Training Details

First, we pre-train a Mask-RCNN with a ResNet50-FPN backbone both on the ApolloCar3D [8] benchmark and the CityScapes [6] benchmark through a car instance segmentation task. Then, we initialize the main backbone by copying the parameters of the pre-trained network. Simultaneously, we pre-train the auxiliary backbone on the COCO dataset using the same network architecture. Finally, we fix the parameters of these two backbones to train the network on the augmented data. The multi-task loss is defined as:

$$L = L_{class}^p + L_{reg}^p + L_{class}^r + L_{box}^r + L_{mask}^r + L_{state}^r + L_{part}^r, \quad (5)$$

TABLE 1

The constructed VUS dataset, which annotates 1850 car instances in uncommon states from 1441 street-view images. “fl-o. (br-o.)” indicates an opened front-left (back-right) part, and “l-tu. (r-tu.)” indicates turning left (right).

Datasets	Bonnet	Trunk	Doors				Headlights		Taillights				Total
	lifted	lifted	fl-o.	fr-o.	bl-o.	br-o.	l-tu.	r-tu.	l-tu.	r-tu.	stop	alarm	
<i>KITTI</i>	1	9	1	0	0	5	1	0	2	1	8	0	28
<i>CityScapes</i>	0	0	14	5	8	4	3	2	4	0	15	0	55
<i>ApolloScape</i>	0	23	29	0	59	157	15	18	23	27	33	16	400
<i>ApolloCar3D</i>	0	13	19	1	0	11	3	5	12	9	21	0	94
<i>Capt. Images</i>	15	405	232	66	79	346	19	17	25	18	44	7	1273
VUS Dataset	16	450	295	72	146	523	41	42	66	55	121	23	1850

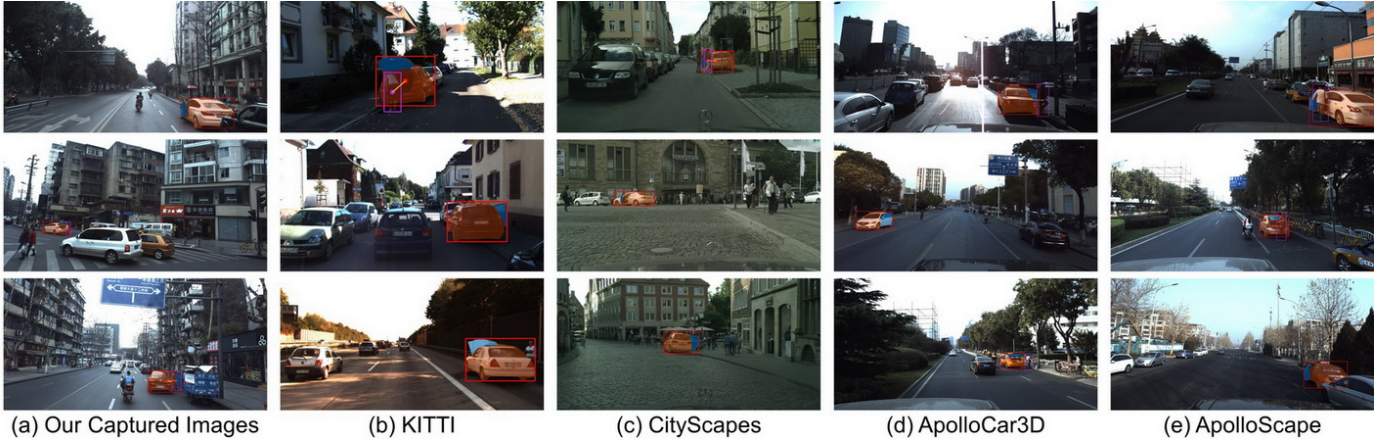


Fig. 8. Samples of our constructed VUS dataset. For each 2D instance of VUS, we manually label its 2D bounding box (with red color), instance segmentation (with orange color), dynamic part segmentation (with blue color), and state description. If there exist human interactions, we add the human bounding box (with pink color), the connection between the center points of the human and the vehicle (with yellow line), as well as the interaction semantics. We capture the majority of the source images (a). Only a few source images are from the popular public AD datasets, including: (b) KITTI; (c) CityScapes; (d) ApolloCar3D; and (e) ApolloCar3D.

where $(\cdot)^p$ and $(\cdot)^r$ indicate RPN and RCNN, respectively. The subscripts *state* and *part* denote the loss of state vector and part mask, respectively. We minimize our loss function using the SGD with a weight decay of 0.0001 and a momentum of 0.9. The learning rate is initially set to 0.002 and reduced by 0.1 for every 5 epochs.

3.3 Multi-Stream Network for VHI Parsing

The proposed two-backbone network in Sec. 3.2 is used to detect, segment, and parse the VUS. However, we notice that some VUS cases contain human interaction. Inevitably, if the vehicle is occluded by humans, it will degrade the network performance. To increase the safety of the AD and improve the perception performance, we present a multi-stream fusion network designed for inferring the vehicle-human interaction semantics, which is shown in Fig. 7. Specifically, we first utilize a human stream and a vehicle stream to extract human and vehicle features, respectively. Meanwhile, spatial maps [54] and human pose maps [54], [55] are also computed. We fuse these four streams to infer the interaction semantics between humans and vehicles.

Human Stream. We extract human appearance ROI pooling features using the Mask-RCNN [3] network, then feed those features into the convolutional layer (H_c) to get the feature f_h . Then we employ pose estimation [3] to estimate its 17 key-points (COCO format [28]). These key-points’ 2D coordinates are reorganized into a 34-dimension

vector that is rescaled to [0,1]. We exploit two 256 sized FCs to extract the pose feature f_p .

Vehicle Stream. We further use the CUS parsing network (Sec. 3.2) to extract the basic vehicle appearance ROI pooling features. In addition, we obtain high-level multi-task branch features. State description branch output is used to infer specific interaction patterns.

Spatial Stream. Spatial stream is used to encode the spatial location of objects and humans. Candidate objects and human bounding boxes are encoded to a binary two-channel tensor, as in previous methods [54], [55]. Intuitively, such a human-object bounding box pair gives important cues for inferring interactive or non-interactive states, *e.g.*, if a person is close to an object, it is very likely that they interact with each other. However, in urban street scenarios, there are many pedestrians around the vehicle, making it difficult to determine the real interactions. Therefore, we encode the vehicle dynamic part into an extra binary channel, which implies many more priors. These three channel tensors are fed into a convolutional layer (S_c) to get the feature f_s . Then we fuse other stream features to determine interactivity.

4 VUS DATASET

To the best of our knowledge, none of the existing datasets provide detailed annotation of *vehicles in uncommon states* (VUS). To evaluate the quality of synthetic data and benchmark network performance, we construct a VUS dataset

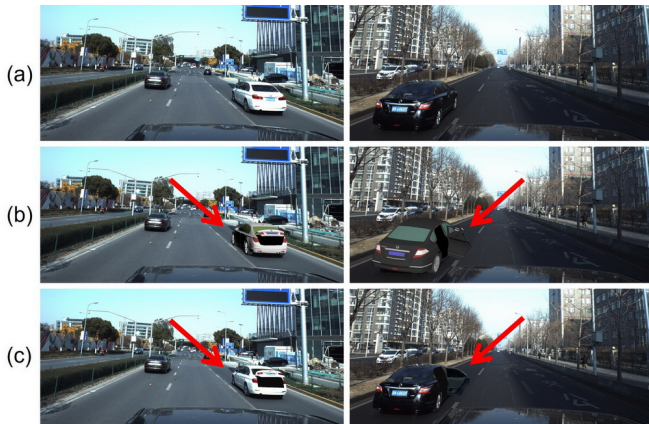


Fig. 9. The training data of baseline methods and ours: (a) raw images; (b) rendering data; (c) synthetic data by our approach.

with annotated real street-view images. Specifically, we first look up the existing AD-oriented datasets, including KITTI [5], CityScapes [6], ApolloScape [7], and Apollo-Car3D [8]. These four datasets have a total of 80,000 images and over 1 million labeled car instances. However, very few of them are in uncommon states (Tab. 1).

To add more VUS data, we drive a car to capture images in various sites (*i.e.*, hospital, park, school, and urban road) and in different timeframes (*i.e.* morning, noon, and afternoon). We capture about 150,000 images in total. After removing the blurred and overexposed images, we finally collect 1273 car instances to label.

As shown in Tab. 1, our dataset covers **10** dynamic parts (*i.e.* the bonnet, the trunk, four doors, two headlights, and two taillights) and **12** uncommon states, which produces **1850** annotated car instances from **1441** images. For each car instance, we manually label the 2D bounding box, instance segmentation, dynamic part segmentation, and state description. If there exist human interactions, we annotate the human bounding box, the connection between the center points of the human and the vehicle, as well as the VHI semantics (*e.g.*, getting on/out, placing/removing luggage, etc). Note that our trained deep model is used directly for testing on VUS dataset without any “domain adaptation” or “fine-tuning” strategies. We believe the built benchmark can effectively verify the quality of augmented data and quantitatively evaluate the network performance.

5 EXPERIMENTS AND DISCUSSION

In this section, we first introduce the experimental settings and computation time. Then we describe the evaluation metric and baseline methods for comparison and present a discussion. Next, we conduct an ablation study to justify the effectiveness of our data augmentation pipeline. Furthermore, we conduct experiments to analyze the system performance, including network structure, training data number, and the rendering factors. Next, we conduct various qualitative experiments to demonstrate the generalizability of our approach.

TABLE 2

Comparison with five baseline methods on 2D detection and instance segmentation on the VUS dataset. All of the numbers are the higher the better. From this table, we can see that our approach advances other baseline methods by a big margin (over 8 percentage points).

Methods	2D Detection (<i>IoU</i>)	Instance Seg. (<i>IoU</i>)
Baseline 1	0.751	0.704
Baseline 2	0.758	0.712
Baseline 3	0.775	0.721
Baseline 4	0.766	0.713
Baseline 5	0.772	0.719
Ours	0.862	0.815

5.1 Experimental Settings and Computation Time

Our network is trained on a 64-bit workstation with an 8-core 3.4 GHz CPU, 4 Nvidia TITAN XP graphics cards, and Ubuntu 16.04 OS. The generated training data mostly comes from the ApolloCar3D dataset, which labels the 3D model and 6-DoF pose for each car instance. Considering the obvious domain gap among different datasets, we further annotate 100 common car instances with 2D-3D aligned in KITTI, CityScapes, ApolloScape, and captured images. Then we perform the proposed data augmentation approach to generate VUS data for training. The processing runtime for each car is about 3 seconds: 0.5s for 3D points transformation and projection, 0.5s for hole filling and filtering, and 2s for invisible region generation.

The training time of our network depends on the data number. In general, training 25K images takes 24 hours. In the testing phase, we directly use the trained model to perform fine-grained understanding on the VUS dataset. As shown in Fig. 1, 13, 16, 17, our network outputs holistic parsing results, including 2D detection, instance-level segmentation, dynamic part segmentation, state description, and VHI semantics. The source code, the dataset, and more results will be found on the project page.

5.2 Evaluation Metric

In Sec. 5.3.1, our network is compared with Mask-RCNN. Note that the proposed benchmark is only focused on VUS. While Mask-RCNN cannot distinguish between the vehicles in *common/uncommon* states, which both exist in the testing data. If we use the *AP* metric to evaluate this experiment, the detected common-state cars will decrease the precision, resulting in an inaccurate *AP* value. Therefore, we compute the maximum number of *IoU* values between the ground truth and the predictions to evaluate the network performance.

Different from Mask-RCNN, our two-backbone network can correctly detect vehicles in uncommon states. For the ablation study in Sec. 5.4 and the performance analysis in Sec. 5.5, we choose the *mAP* metric to evaluate the performance of 2D detection, instance level segmentation, and dynamic part segmentation. For state description, we compute the match rate at each binary item between prediction state vectors and the ground truth.

TABLE 3

Ablation study of our data augmentation pipeline. All numbers are the higher the better. From the table, we can see that our VUS network and VHI network trained by VUS data and VHI data get the best performance on the tasks of fine-grained vehicle perception.

Fine-Grained Vehicle Perception	VUS Parsing				VHI Parsing	
	Detection	Instance Seg.	Part Seg.	State Desc.	Detection	Semantics
VUS Data	0.632	0.485	/	/	/	/
VUS Data + VUS Network	0.701	0.563	0.314	0.874	/	/
VUS Data + VHI Data + VUS Network	0.733	0.581	0.345	0.893	/	/
VUS Data + VHI Data + VUS Network + VHI Network	0.733	0.581	0.345	0.893	0.678	0.562

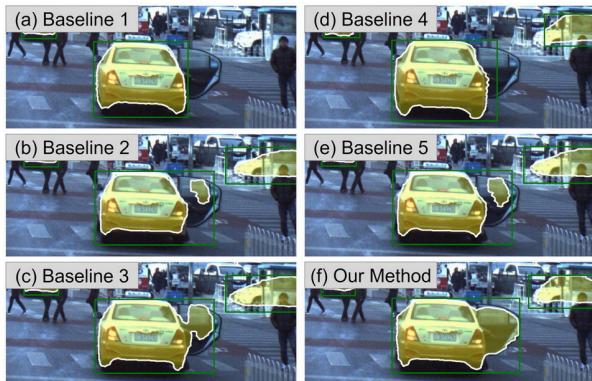


Fig. 10. Visualization results on 2D detection and instance segmentation (five baseline methods vs. ours).

5.3 Comparisons

5.3.1 Comparison on the VUS Parsing Task

To demonstrate that our method can effectively improve the performance on 2D detection and instance-level segmentation, the following baseline methods are compared (Tab. 2):

Baseline 1: Mask-RCNN + Existing Datasets. We train the Mask-RCNN network on the existing datasets (*i.e.*, KITTI, CityScapes, ApolloScape, and ApolloCar3D), which only annotate the common-state cars (Fig. 9 (a)). In the testing phase, we directly output the results of 2D detection and instance-level segmentation on the VUS dataset.

Baseline 2: Mask-RCNN + Rendering Data. We implement the rendering-based data generation pipeline which is adopted in most image synthesis works [11], [12], [40]. Following [10], we construct 50 high-quality textured CAD models of cars, which are labeled on the dynamic parts and motion axis. We transform the car models according to the 6-DoF pose and operate the dynamic parts to generate uncommon states. Here, we use *Blender* software to obtain a rendering result that is further overlaid on the background (Fig. 9 (b)). Consequently, we build a rendering dataset consisting of 25K images. We train the Mask-RCNN network on the rendering data and test on the VUS dataset.

Baseline 3: Mask-RCNN + Our Synthetic Data. We then train the Mask-RCNN network using our synthetic data (Fig. 9 (c)), which has the same number as the rendering data. We evaluate it on the VUS dataset.

Baseline 4: Our Network + Existing Datasets. We train our two-backbone network using the existing datasets which are introduced in *Baseline 1*.

Baseline 5: Our Network + Rendering Data. We train the proposed two-backbone network using the rendering data

TABLE 4

Comparison with Faster-RCNN-based HOI detection method.

Tasks	Faster-RCNN	Ours
VHI Detection (<i>mAP</i>)	0.634	0.678
VHI Description (<i>mAP</i>)	0.432	0.562

which is illustrated in *Baseline 2*.

Our method: Our Network + Our Synthetic Data. Finally, we train our two-backbone network using our synthetic data. The quantitative results of these approaches are listed in Tab. 2.

The results of *Baseline 1* indicate that the model of Mask-RCNN trained by common-state cars can detect and segment the car body. However, the dynamic parts are always ignored (Fig. 10 (a)). The results of *Baseline 2* show that rendering data improves the network performance compared with *Baseline 1*. The rendering data (Fig. 9 (b)) has the natural domain gap with the real captured images (Fig. 9 (a)). In addition, 3D rendering costs much more than 10x our data augmentation approach. The results of *Baseline 3* prove that Mask-RCNN trained by our synthetic data outperforms existing datasets and rendering data. However, when we visualize the results of detection and segmentation in Fig. 10 (c), it is shown that the visible parts are good while the reverse side of the dynamic part suffers from errors.

Baseline 4 and *Baseline 5* are using our two-backbone network to train on the existing datasets and rendering data, respectively. However, the performances of both baseline methods are not improved significantly. Here, we emphasize that our two-backbone network is carefully designed to learn our synthetic data, especially the dynamic parts. Directly using our network cannot effectively learn other data, because they are in different domains. Consequently, our two-backbone network trained by synthetic data gets the best performance, which advances other methods by over 8 percent on both tasks (Tab. 2). The main improvement comes from the invisible regions (Fig. 10 (f)).

5.3.2 Comparison on the VHI Parsing Task

We use the VUS parsing network (Sec. 3.2) as a detector to extract the input of the VHI network. Compared with the Faster-RCNN-based method, it can provide more information about the locations of the movable parts and the detailed state descriptions of VUS, which are important cues for VHI detection and detailed VHI description. In this experiment, our VHI parsing approach is compared with the Faster-RCNN-based method. We quantitatively

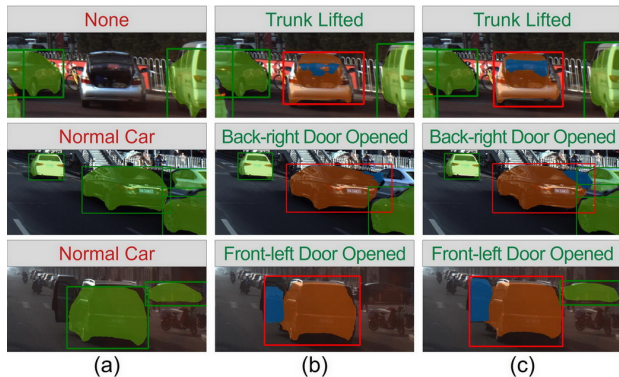


Fig. 11. Visual results on the ablation study of our network: (a) single backbone re-trained; (b) single backbone frozen; (c) two backbones frozen. The words in red/green indicate the wrong/correct descriptions.

evaluate these two methods on the VUS dataset by using equal numbers of training data. As shown in Tab. 4, with a movable part location and a detailed car state provided by VUS parsing network, the VHI network achieves 4.4 and 13.0 improvements for interaction reasoning and detailed pattern localization.

5.4 Ablation Study of Our Data Augmentation Pipeline

Our data augmentation pipeline includes four main components: 1) VUS data generation; 2) VHI data generation; 3) multi-task network for VUS parsing; and 4) multi-stream network for VHI parsing. To justify the effectiveness of each component, we conduct an ablation study on the tasks of fine-grained vehicle perception. As depicted in Tab. 3, we first use the VUS data to train a Mask-RCNN network, which is used as a baseline method (the second row). Then we train the VUS network using the VUS data (the third row). This approach not only can perform the tasks of part-level segmentation and state description, but also effectively improves 2D detection and instance-level segmentation tasks by 6.9 and 7.8 percentage points, respectively. Next, we use the VHI data and the VUS data to train the VUS network (the fourth row). It is shown that VHI data improves the network performance (*i.e.* [15]) on 2D detection, instance-level segmentation, part-level segmentation, and state description by 3.2, 1.8, 3.1, and 1.9 percentage points, respectively. Based on the VUS data and VHI data, we further train the VHI network to parse the vehicle-human interactions (the fifth row). The results of VHI detection and VHI semantics are 67.8 and 56.2 percentage points, respectively. From this ablation study, we can find that our data augmentation pipeline is robust and effective for fine-grained vehicle perception.

5.5 Performance Analysis

5.5.1 The Impact of Our Network Structure

In addition to 2D detection and instance segmentation, our network can detect vehicles in uncommon states, segment dynamic parts, and describe states. To illustrate the impact of our network structure, we conduct an ablation study as shown in Tab. 5 using a constant number of training data (*i.e.* 25K). We first re-train the single backbone, which is

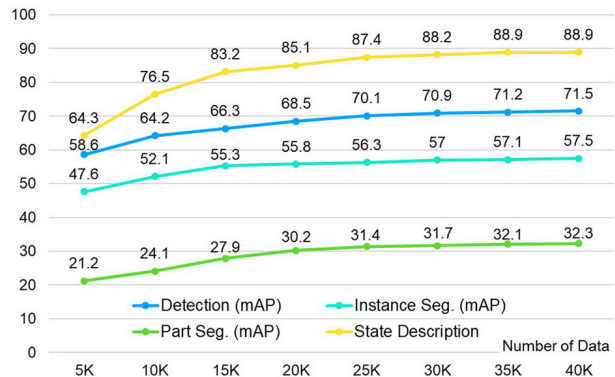


Fig. 12. The performance of our two-backbone network with different numbers of training data.

TABLE 5

Ablation study of our network on 2D detection, instance segmentation, part segmentation, and state description. “S. B. Retrained” indicates single backbone retained, “S. B. Frozen” means single backbone frozen, and “T. B. Frozen” indicates two backbones frozen. We see that the strategy of two backbones frozen gets the best performance.

Tasks	S. B. Retrained	S. B. Frozen	T. B. Frozen
Detection (<i>mAP</i>)	0.136	0.672	0.701
Ins. Seg. (<i>mAP</i>)	0.114	0.516	0.563
Part Seg. (<i>mAP</i>)	0.144	0.273	0.314
State Description	0.149	0.837	0.874

a common strategy in most deep networks (*e.g.*, [3]). The results show that it is barely able to predict the correct class of VUS, leading to bad performance on these tasks (Fig. 11 (a)). We then freeze the single backbone pre-trained on COCO during the synthetic data training. The performance is improved because we have relieved the over-fitting problem. However, the frozen backbone cannot extract adequate features (Fig. 11 (b)). In contrast, our two backbones, which pre-trained on a car detection task and a general task can not only extract adequate features but also avoid the over-fitting problem. It achieves the best performance on these tasks (Fig. 11 (c)).

5.5.2 The Impact of the Number of Training Data

Empirically, the performance of deep networks largely relies on the number of training data. Here, we conduct an experiment to study the relationship between the number of data and network performance. Thanks to the fully automatic data augmentation approach, we set the number of data from 5K to 40K with an interval of 5K to train our network. Fig. 12 shows the network performance on multiple tasks with respect to different numbers of training data. We find that from 5K to 25K, the network performance is significantly improved. From 25K to 40K, however, the network is not sensitive to the number of training data. There are two main reasons: 1) network capability. We cannot always improve the network performance by adding the number of training data; 2) test data. There exist some features or cases in the test data those are not well learned by the network. In practice, we set the number of training data to 25K, which is a good compromise of efficiency and accuracy.



Fig. 13. Fine-grained parsing results of VUS and VHI by our approach in three video sequences of street-view images.

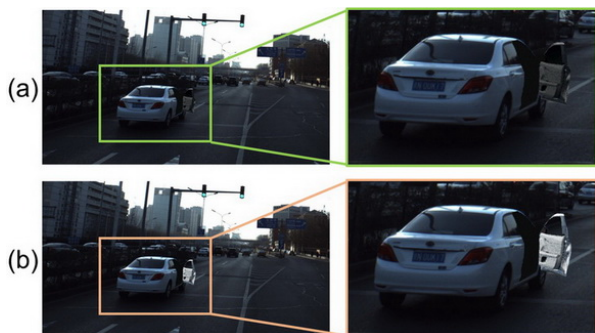


Fig. 14. The rendering results with (a) and without (b) environment map.

TABLE 6

The impact of the environment map. The table shows that the environment map significantly improves the network performance. In particular, the dynamic part segmentation gets a 9.3 percent improvement.

Tasks	w/o Env. Map	with Env. Map
2D Detection (mAP)	0.688	0.701
Ins. Seg. (mAP)	0.538	0.563
Part Seg. (mAP)	0.221	0.314
State Description	0.844	0.874

5.5.3 The Impact of the Environment Map

In the proposed data generation pipeline, we render the reverse sides of dynamic parts to generate the invisible region data. In the wild, illumination (or an environment map) plays an important role in determining whether the rendered region is compatible with the surroundings. Here, we conduct an experiment to study the effectiveness of environment maps. We utilize the same number of reverse side data with/without an environment map (shown in Fig. 14) to train our network and evaluate it on the proposed VUS dataset. As shown in Tab. 6, the data rendered by the environment map significantly improves the network performance. In particular, the dynamic part segmentation is improved by 9.3 percent.



Fig. 15. More synthetic results of vehicles by our approach. The vehicles' types include truck, bus, and van.

5.6 Qualitative Evaluation

It is essential to conduct quantitative evaluations and comparisons as in Sec. 5.3, Sec. 5.4, and Sec. 5.5. However, for AD, robustness and generalizability are the most critical issues. In this section, we conduct various qualitative experiments to demonstrate the effectiveness of our approach.

5.6.1 Generalizability of Our Approach

Our data augmentation approach is generic and can be transferred to other objects such as the human body and furniture. These objects are constructed by parts, and each part has a corresponding motion axis. Based on the 2D-3D alignment datasets, ApolloCar3D (vehicle), Unite the People (human body), and Pixel3D (furniture), we can generate diverse results using our approach. In this paper, we focus on vehicle augmentation and perception. Fig. 15 shows the synthetic results of different vehicle types, such as truck, bus, and van.



Fig. 16. Fine-grained parsing results of VUS and VHI by our method in different sites: (a) the side of the road; (b) the crossroads.



Fig. 17. Fine-grained parsing results of VUS and VHI by our method in different cities: (a) Beijing; (b) Shanghai; (c) Chengdu; (d) Guangzhou.

5.6.2 Fine-grained Parsing on Video Sequence

Fig. 13 shows the fine-grained perception results produced by our approach in three different sequences of street-view images. The common vehicles are shown in green, which can be obtained by conventional methods of detection and segmentation. In contrast, our approach can perceive the VUS cases (with red bounding boxes) as well as the VHI cases (with pink bounding boxes). Both are important for the safety of the autonomous vehicle. It is clear that accurate and robust instance segmentation results can be estimated by our network. Note that these images are captured by a moving car, which is different from our training data. The results are generated without network “re-training” or “fine-tuning”, which justifies the advantages of our approach.

5.6.3 Parsing Results on Different Sites

In Fig. 16, we demonstrate the fine-grained vehicle perception results on different sites, particularly the side of the road and the crossroads. Usually, vehicles are not allowed to stop at these sites with doors/trunks open for getting

in/out or placing/removing luggage. However, we still find a number of dangerous behaviors from drivers and pedestrians. Our approach can perceive these VUS cases and VHI cases in advance, which is very important for the planning and decision modules of AD systems.

5.6.4 Parsing Results on Different Cities

To demonstrate the robustness and generalizability of our approach, we conduct experiments in various cities, which have different weathers, different buildings, different roads, and different plants. Fig. 17 shows the fine-grained vehicle perception results for different cities, including Beijing, Shanghai, Chengdu, and Guangzhou. Note that these source images are different from the training data and our network is not “re-trained” or “fine-tuned” to fit the test data. From this experiment, we find that VUS cases and VHI cases vary wildly in the traffic scenarios. Our approach fills the missing piece by providing detailed vehicle parsing and “vehicle - human” interaction semantics.

6 CONCLUSION AND LIMITATION

In this paper, we make the first attempt to analyze vehicles in uncommon states (VUS). Instead of annotating a large number of images, we present a visual data augmentation approach that takes advantage of 3D parts. Our method is light-weight but high-efficiency, which advances the rendering-based methods by a large margin. To perform a holistic understanding for VUS, we propose a multi-task deep network that can simultaneously output 2D detection, instance-level segmentation, dynamic part segmentation, and state description. Moreover, we design a multi-stream fusion network to parse the VHI semantics. To benchmark the performance, we construct a VUS dataset containing 1441 real images (1850 car instances) with fine-grained annotation. The experimental results show that our synthetic data and the proposed deep network perform well on VUS.

Nevertheless, there are a number of limitations, which we will tackle in future work. First, the uncommon states analyzed in this paper are limited to vehicles. Some other objects, such as buildings and roads, require more attention. Second, the outputs of our network are mostly 2D results. We will extend this work to the 3D space, using 3D detection, 3D localization, and 3D reconstruction. Finally, we will research VUS and VHI on the video sequences and multiple sensors fusion data (e.g., cameras, Lidar, and Radar).

ACKNOWLEDGEMENT

This work was supported in part by National Natural Science Foundation of China (U1736217 and 61932003), National Key R&D Program of China (2019YFF0302902), and Pre-research Project of the Manned Space Flight (060601).

REFERENCES

- [1] S. Ren, K. He, R. Girshick, and J. Sun, "Faster r-cnn: Towards real-time object detection with region proposal networks," in *Advances in Neural Information Processing Systems*, 2015, pp. 91–99.
- [2] C.-Y. Fu, W. Liu, A. Ranga, A. Tyagi, and A. C. Berg, "Dssd: Deconvolutional single shot detector," *arXiv preprint arXiv:1701.06659*, 2017.
- [3] K. He, G. Gkioxari, P. Dollár, and R. Girshick, "Mask r-cnn," in *Proceedings of the IEEE International Conference on Computer Vision*, 2017, pp. 2961–2969.
- [4] C. Lu, H. Su, Y. Li, Y. Lu, L. Yi, C.-K. Tang, and L. J. Guibas, "Beyond holistic object recognition: Enriching image understanding with part states," in *Proceedings of the IEEE Conference on Computer Vision and Pattern Recognition*, 2018, pp. 6955–6963.
- [5] A. Geiger, P. Lenz, C. Stiller, and R. Urtasun, "Vision meets robotics: The kitti dataset," *The International Journal of Robotics Research*, vol. 32, no. 11, pp. 1231–1237, 2013.
- [6] M. Cordts, M. Omran, S. Ramos, T. Rehfeld, M. Enzweiler, R. Benenson, U. Franke, S. Roth, and B. Schiele, "The cityscapes dataset for semantic urban scene understanding," in *Proceedings of the IEEE Conference on Computer Vision and Pattern Recognition*, 2016, pp. 3213–3223.
- [7] X. Huang, X. Cheng, Q. Geng, B. Cao, D. Zhou, P. Wang, Y. Lin, and R. Yang, "The apollo scape dataset for autonomous driving," in *Proceedings of the IEEE Conference on Computer Vision and Pattern Recognition Workshops*, 2018, pp. 954–960.
- [8] X. Song, P. Wang, D. Zhou, R. Zhu, C. Guan, Y. Dai, H. Su, H. Li, and R. Yang, "Apollocar3d: A large 3d car instance understanding benchmark for autonomous driving," in *Proceedings of the IEEE Conference on Computer Vision and Pattern Recognition*, 2019, pp. 5452–5462.
- [9] R. Geirhos, P. Rubisch, C. Michaelis, M. Bethge, F. A. Wichmann, and W. Brendel, "Imagenet-trained cnns are biased towards texture; increasing shape bias improves accuracy and robustness," *arXiv preprint arXiv:1811.12231*, 2018.
- [10] H. A. Alhaja, S. K. Mustikovela, L. Mescheder, A. Geiger, and C. Rother, "Augmented reality meets computer vision."
- [11] J. Tremblay, A. Prakash, D. Acuna, M. Brophy, V. Jampani, C. Anil, T. To, E. Cameracci, S. Boochoon, and S. Birchfield, "Training deep networks with synthetic data: Bridging the reality gap by domain randomization," in *Proceedings of the IEEE Conference on Computer Vision and Pattern Recognition Workshops*, 2018, pp. 969–977.
- [12] A. Prakash, S. Boochoon, M. Brophy, D. Acuna, E. Cameracci, G. State, O. Shapira, and S. Birchfield, "Structured domain randomization: Bridging the reality gap by context-aware synthetic data," *arXiv preprint arXiv:1810.10093*, 2018.
- [13] M. Loper, N. Mahmood, J. Romero, G. Pons-Moll, and M. J. Black, "Smpl: A skinned multi-person linear model," *ACM transactions on graphics (TOG)*, vol. 34, no. 6, pp. 1–16, 2015.
- [14] M. Kocabas, N. Athanasiou, and M. J. Black, "Vibe: Video inference for human body pose and shape estimation," in *Proceedings of the IEEE/CVF Conference on Computer Vision and Pattern Recognition*, 2020, pp. 5253–5263.
- [15] Z. Liu, F. Lu, P. Wang, H. Miao, L. Zhang, R. Yang, and B. Zhou, "3d part guided image editing for fine-grained object understanding," in *Proceedings of the IEEE/CVF Conference on Computer Vision and Pattern Recognition*, 2020, pp. 11 336–11 345.
- [16] G. J. Brostow, J. Fauqueur, and R. Cipolla, "Semantic object classes in video: A high-definition ground truth database," *Pattern Recognition Letters*, vol. 30, no. 2, pp. 88–97, 2009.
- [17] S. Wang, M. Bai, G. Mattyus, H. Chu, W. Luo, B. Yang, J. Liang, J. Cheverie, S. Fidler, and R. Urtasun, "Torontocity: Seeing the world with a million eyes," *arXiv preprint arXiv:1612.00423*, 2016.
- [18] G. Neuhold, T. Ollmann, S. Rota Buló, and P. Kotschieder, "The mapillary vistas dataset for semantic understanding of street scenes," in *Proceedings of the IEEE International Conference on Computer Vision*, 2017, pp. 4990–4999.
- [19] F. Yu, W. Xian, Y. Chen, F. Liu, M. Liao, V. Madhavan, and T. Darrell, "Bdd100k: A diverse driving video database with scalable annotation tooling," *arXiv preprint arXiv:1805.04687*, 2018.
- [20] G. Ros, L. Sellart, J. Materzynska, D. Vazquez, and A. M. Lopez, "The synthia dataset: A large collection of synthetic images for semantic segmentation of urban scenes," in *Proceedings of the IEEE Conference on Computer Vision and Pattern Recognition*, 2016, pp. 3234–3243.
- [21] S. R. Richter, Z. Hayder, and V. Koltun, "Playing for benchmarks," in *Proceedings of the IEEE International Conference on Computer Vision*, 2017, pp. 2213–2222.
- [22] F. Engelmann, T. Kontogianni, A. Hermans, and B. Leibe, "Exploring spatial context for 3d semantic segmentation of point clouds," in *Proceedings of the IEEE International Conference on Computer Vision*, 2017, pp. 716–724.
- [23] A. Krizhevsky, I. Sutskever, and G. E. Hinton, "Imagenet classification with deep convolutional neural networks," in *Advances in Neural Information Processing Systems*, 2012, pp. 1097–1105.
- [24] K. Simonyan and A. Zisserman, "Very deep convolutional networks for large-scale image recognition," *arXiv preprint arXiv:1409.1556*, 2014.
- [25] K. He, X. Zhang, S. Ren, and J. Sun, "Deep residual learning for image recognition," in *Proceedings of the IEEE Conference on Computer Vision and Pattern Recognition*, 2016, pp. 770–778.
- [26] T.-Y. Lin, P. Dollár, R. Girshick, K. He, B. Hariharan, and S. Belongie, "Feature pyramid networks for object detection," in *Proceedings of the IEEE Conference on Computer Vision and Pattern Recognition*, 2017, pp. 2117–2125.
- [27] J. Deng, W. Dong, R. Socher, L.-J. Li, K. Li, and L. Fei-Fei, "Imagenet: A large-scale hierarchical image database," in *Proceedings of the IEEE Conference on Computer Vision and Pattern Recognition*. IEEE, 2009, pp. 248–255.
- [28] T.-Y. Lin, M. Maire, S. Belongie, J. Hays, P. Perona, D. Ramanan, P. Dollár, and C. L. Zitnick, "Microsoft coco: Common objects in context," in *Proceedings of ECCV*. Springer, 2014, pp. 740–755.
- [29] D. Dwivedi, I. Misra, and M. Hebert, "Cut, paste and learn: Surprisingly easy synthesis for instance detection," in *Proceedings of the IEEE International Conference on Computer Vision*, 2017, pp. 1301–1310.
- [30] A. X. Chang, T. Funkhouser, L. Guibas, P. Hanrahan, Q. Huang, Z. Li, S. Savarese, M. Savva, S. Song, H. Su, J. Xiao, L. Yi, and F. Yu, "ShapeNet: An Information-Rich 3D Model Repository," Tech. Rep. arXiv:1512.03012 [cs.GR], 2015.
- [31] Z. Wu, S. Song, A. Khosla, F. Yu, L. Zhang, X. Tang, and J. Xiao, "3d shapenets: A deep representation for volumetric shapes," in

- Proceedings of the IEEE Conference on Computer Vision and Pattern Recognition*, 2015, pp. 1912–1920.
- [32] A. Dai, A. X. Chang, M. Savva, M. Halber, T. Funkhouser, and M. Nießner, “Scannet: Richly-annotated 3d reconstructions of indoor scenes,” in *Proceedings of the IEEE Conference on Computer Vision and Pattern Recognition*, 2017.
- [33] D. J. Butler, J. Wulff, G. B. Stanley, and M. J. Black, “A naturalistic open source movie for optical flow evaluation,” in *Proceedings of ECCV*. Springer, 2012, pp. 611–625.
- [34] A. Dosovitskiy, P. Fischer, E. Ilg, P. Hausser, C. Hazirbas, V. Golkov, P. Van Der Smagt, D. Cremers, and T. Brox, “FlowNet: Learning optical flow with convolutional networks,” in *Proceedings of the IEEE International Conference on Computer Vision*, 2015, pp. 2758–2766.
- [35] N. Mayer, E. Ilg, P. Hausser, P. Fischer, D. Cremers, A. Dosovitskiy, and T. Brox, “A large dataset to train convolutional networks for disparity, optical flow, and scene flow estimation,” in *Proceedings of the IEEE Conference on Computer Vision and Pattern Recognition*, 2016, pp. 4040–4048.
- [36] W. Qiu and A. Yuille, “Unrealcv: Connecting computer vision to unreal engine,” in *Proceedings of ECCV*. Springer, 2016, pp. 909–916.
- [37] Y. Zhang, W. Qiu, Q. Chen, X. Hu, and A. Yuille, “Unrealstereo: A synthetic dataset for analyzing stereo vision,” *arXiv preprint arXiv:1612.04647*, vol. 1, no. 2, 2016.
- [38] S. R. Richter, V. Vineet, S. Roth, and V. Koltun, “Playing for data: Ground truth from computer games,” in *Proceedings of ECCV*. Springer, 2016, pp. 102–118.
- [39] S. Suwajanakorn, N. Snavely, J. J. Tompson, and M. Norouzi, “Discovery of latent 3d keypoints via end-to-end geometric reasoning,” in *Advances in Neural Information Processing Systems*, 2018, pp. 2059–2070.
- [40] H. Su, C. R. Qi, Y. Li, and L. J. Guibas, “Render for cnn: Viewpoint estimation in images using cnns trained with rendered 3d model views,” in *Proceedings of the IEEE International Conference on Computer Vision*, 2015, pp. 2686–2694.
- [41] M. Müller, V. Casser, J. Lahoud, N. Smith, and B. Ghanem, “Sim4cv: A photo-realistic simulator for computer vision applications,” *International Journal of Computer Vision*, vol. 126, no. 9, pp. 902–919, 2018.
- [42] A. Handa, V. Patraucean, V. Badrinarayanan, S. Stent, and R. Cipolla, “Understanding real world indoor scenes with synthetic data,” in *Proceedings of the IEEE Conference on Computer Vision and Pattern Recognition*, 2016, pp. 4077–4085.
- [43] A. Gaidon, Q. Wang, Y. Cabon, and E. Vig, “Virtual worlds as proxy for multi-object tracking analysis,” in *Proceedings of the IEEE Conference on Computer Vision and Pattern Recognition*, 2016, pp. 4340–4349.
- [44] J. Tobin, R. Fong, A. Ray, J. Schneider, W. Zaremba, and P. Abbeel, “Domain randomization for transferring deep neural networks from simulation to the real world,” in *International Conference on Intelligent Robots and Systems (IROS)*. IEEE, 2017, pp. 23–30.
- [45] S. Hinterstoisser, V. Lepetit, P. Wohlhart, and K. Konolige, “On pre-trained image features and synthetic images for deep learning,” in *The European Conference on Computer Vision (ECCV) Workshops*, September 2018.
- [46] J. Redmon and A. Farhadi, “Yolov3: An incremental improvement,” *arXiv preprint arXiv:1804.02767*, 2018.
- [47] P. Wang, X. Shen, Z. Lin, S. Cohen, B. Price, and A. L. Yuille, “Joint object and part segmentation using deep learned potentials,” in *Proceedings of the IEEE International Conference on Computer Vision*, 2015, pp. 1573–1581.
- [48] F. Xia, P. Wang, L.-C. Chen, and A. L. Yuille, “Zoom better to see clearer: Human and object parsing with hierarchical auto-zoom net,” in *Proceedings of ECCV*. Springer, 2016, pp. 648–663.
- [49] R. W. Sumner, J. Schmid, and M. Pauly, “Embedded deformation for shape manipulation,” *ACM Transactions on Graphics (TOG)*, vol. 26, no. 3, p. 80, 2007.
- [50] C. Tomasi and R. Manduchi, “Bilateral filtering for gray and color images,” in *Proceedings of ICCV*, vol. 98, no. 1, 1998, p. 2.
- [51] J.-F. Lalonde and A. A. Efros, “Synthesizing environment maps from a single image,” *Technical Report CMU-R I-TR-10-24*, 2010.
- [52] R. Alp Güler, N. Neverova, and I. Kokkinos, “Densepose: Dense human pose estimation in the wild,” in *Proceedings of the IEEE Conference on Computer Vision and Pattern Recognition*, 2018, pp. 7297–7306.
- [53] G. Varol, J. Romero, X. Martin, N. Mahmood, M. J. Black, I. Laptev, and C. Schmid, “Learning from synthetic humans,” in *Proceedings of the IEEE Conference on Computer Vision and Pattern Recognition*, 2017, pp. 109–117.
- [54] Y.-W. Chao, Y. Liu, X. Liu, H. Zeng, and J. Deng, “Learning to detect human-object interactions,” in *2018 IEEE winter conference on applications of computer vision (wacv)*. IEEE, 2018, pp. 381–389.
- [55] Y.-L. Li, S. Zhou, X. Huang, L. Xu, Z. Ma, H.-S. Fang, Y. Wang, and C. Lu, “Transferable interactiveness knowledge for human-object interaction detection,” in *Proceedings of the IEEE Conference on Computer Vision and Pattern Recognition*, 2019, pp. 3585–3594.



Feixiang Lu is currently a senior researcher at the Robotics and Autonomous Driving Lab, Baidu Research, Baidu Inc., China. He obtained his Ph.D. degree in Computer Science from Beihang University in 2019. He received the B.S. degree from Beijing University of Posts and Telecommunications in 2013. His research interests include 3D reconstruction, scene parsing, and their applications in autonomous driving. He received the Best Paper Award at the Computer Graphics International (CGI) in 2018.



Zongdai Liu is currently a research intern in Robotics and Autonomous Driving Lab, Baidu Research, Baidu Inc., China. He is also a master student in Beihang University. He received the B.S. degree from Taiyuan University of Technology. His research interests include 3D detection, scene parsing, and their applications in autonomous driving.



Hui Miao is currently a master student in School of Computer Science and Engineering, Beihang University. She received the B.S. degree from Beijing Information Science & Technology University. And her research interests include 3D detection, data augmentation and their applications in autonomous driving.



Peng Wang is currently a senior research scientist at Bytedance. He graduated from UCLA advised by Professor Alan Yuille. Before UCLA, he obtained his B.S and M.S degree on machine intelligence from Peking University. His research interest is especially on perception of autonomous vehicle/moving robot, such as learning depth and segmentation from stereo, monocular videos/images, fusing multiple sensors such as video and LiDAR. He has published over 20 papers on major computer vision and machine learning conferences such as CVPR, ICCV, ECCV and NIPS.



Liangjun Zhang is the lead of Robotics and Autonomous Driving Lab (RAL) of Baidu Research. Dr. Zhang received his PhD in computer science from the University of North Carolina at Chapel Hill and MS/BS from Zhejiang University. He was a NSF computing innovation fellow in the computer science department at Stanford University. His research interests span robotics, autonomous driving, simulation, geometric computing and computer graphics. He has received a number of awards including the Best Paper

Award at the International CAD Conference and the UNC Linda Dykstra Distinguished PhD Dissertation Award.



Bin Zhou is currently an Associate Professor with the State Key Laboratory of Virtual Reality Technology and Systems, School of Computer Science and Engineering, Beihang University. He is also an Associate Professor with Peng Cheng Laboratory, Shenzhen, China. He received his B.S. and Ph.D. degrees in Computer Science from the Beihang University, China, in 2006 and 2014, respectively. His research interests include Computer Graphics, Virtual Reality, Computer Vision and Robotics. He is the

editorial board member of Virtual Reality & Intelligent Hardware. He served on the program committee of multiple conferences and workshops including ISMAR 2019, AsiaHaptics 2020, VRST 2015, ICVRV 2017~2020, ChinaVR 2017~2020. He has received a number of awards including the Best Paper Award at Computer Graphics International 2018.



Ruigang Yang is the CTO of Inceptio. He is a renowned computer vision scientist. He has published over 100 papers with an H-index of 58. He was an Associate Editor for IEEE T-PAMI. He has served as Area Chairs for premium vision conferences (such as ICCV/CVPR), and will serve as a Program Chair for CVPR 2021. He has made a number of world-class scientific research achievements in the field of 3D reconstruction and 3D data analysis. Before joining Inceptio, he served as the chief scientist for 3D

computer vision and led the Robot and Autonomous Driving Laboratory of Baidu Research. Before that, he was a tenured full professor at the University of Kentucky, USA. He holds a PhD in Computer Science from University of North Carolina at Chapel Hill (UNC-CH), a MS in Computer Science from Columbia University, and finished his undergraduate study from Tsinghua University.



Dinesh Manocha is currently the Paul Chrisman Iribe Chair of Computer Science and Electrical & Computer Engineering at the University of Maryland at College Park. Earlier he was the Matthew Mason/Phi Delta Theta Distinguished Professor of Computer Science at the University of North Carolina at Chapel Hill. He co-leads a major research group with more than 20 members on geometric and simulation algorithms with applications to computer graphics, robotics and virtual environments. He has published more than 500

papers in the leading conferences and journals in computer graphics, robotics, computational geometry, databases, multimedia, high performance computing and symbolic computation, and received 16 best paper and time of test awards. He has also served as program committee member or program chair of more than 120 leading conferences in these areas. Moreover, he has given more than 110 invited or keynote talks at conferences and distinguished lectures at other institutions. Manocha has served as a member of the editorial board or guest editor of eleven leading journals in computer graphics, robotics, geometry processing and scientific computing. He is a co-inventor of 9 patents, several of which have been licensed to industry. He has won many awards including NSF Career Award, ONR Young Investigator Award, Sloan Fellowship, IBM Fellowship, SIGMOD IndySort Winner, Honda Research Award, UNC Hettleman Prize, etc. He is a Fellow of ACM, AAAS, AAAI, and IEEE, and received the Distinguished Alumni Award from Indian Institute of Technology, Delhi.